

# Thermal Stability of the Magnetization in Perpendicularly Magnetized Thin Film Nanomagnets

Gabriel D. Chaves-O'Flynn,<sup>1,2</sup> Eric Vanden-Eijnden,<sup>3</sup> D. L. Stein,<sup>1,3</sup> and A. D. Kent<sup>1</sup>

<sup>1</sup>*Department of Physics, New York University, New York, NY 10003, USA*

<sup>2</sup>*Department of Mathematical Sciences, New Jersey Institute of Technology, Newark, NJ, 07102, USA*

<sup>3</sup>*Courant Institute of Mathematical Sciences, New York University, New York, NY 10012, USA*

Understanding the stability of thin film nanomagnets with perpendicular magnetic anisotropy (PMA) against thermally induced magnetization reversal is important when designing perpendicularly magnetized patterned media and magnetic random access memories. The leading-order dependence of magnetization reversal rates are governed by the energy barrier the system needs to surmount in order for reversal to proceed. In this paper we study the reversal dynamics of these systems and compute the relevant barriers using the string method of E, Vanden-Eijnden, and Ren. We find the reversal to be often spatially incoherent; that is, rather than the magnetization flipping as a rigid unit, reversal proceeds instead through a soliton-like domain wall sweeping through the system. We show that for square nanomagnetic elements the energy barrier increases with element size up to a critical length scale, beyond which the energy barrier is constant. For circular elements the energy barrier continues to increase indefinitely, albeit more slowly beyond a critical size. In both cases the energy barriers are smaller than those expected for coherent magnetization reversal.

Thin film elements with perpendicular magnetic anisotropy (PMA) can have magnetization directions that are thermally stable at room temperature at the nanometer scale, a feature that makes them useful in information storage and processing, for example in patterned media [1] and spin-transfer MRAM [2]. A key issue in determining stability is how the energy barriers and transition states of these elements depend on their lateral size. For elements larger than the exchange length (typically  $\sim 5$  nm in transition metal ferromagnets) the assumption of coherent reversal of the magnetization breaks down and the transition state is not uniformly magnetized. Due to the multiscale character of micromagnetism, analytical calculations are complicated and transition states have been calculated only for a handful of physical systems [3–5]. Numerical calculations are usually necessary for the majority of systems. In this paper, we use the string method [6] to find the transition states and activation energies in thin film elements with PMA.

Transition state theory indicates that reversal occurs through states corresponding to critical points of the magnetization energy functional, where  $\nabla_{\mathbf{M}}E = 0$ . The probability for thermally induced magnetization reversal is expected to follow the Arrhenius law  $e^{-U/k_B T}$  where  $U$  is the energy difference between the transition state and the metastable configuration [7]. Here, we identify the minimum energy paths (MEPs) on the energy landscape, which allow us to determine the transition states; we then study the dependence of these states, along with their corresponding energy barriers, on sample size and geometry. Our two main conclusions are: (i) typically, models that assume uniform magnetization seriously overestimate the magnitude of the activation energy, especially in larger systems; and (ii) even in situations where the assumption of uniform magnetization is valid, that is, in smaller size systems, finite size effects have a strong impact on the value of the energy barrier.

The micromagnetic energy of this system is given by [8]:

$$E = \int_V \left[ A |\nabla \mathbf{m}|^2 - K m_z^2 - \mu_0 M_s H_z m_z \right] d^3 \mathbf{r} + E_{\text{dd}} \quad (1)$$

Here  $\mathbf{m}$  is the normalized magnetization vector at positions  $\mathbf{r}$  and the integral is evaluated over the sample volume  $V = \Omega t$ , where  $\Omega$  is the cross sectional area of the sample and  $t$  its thickness. The first term under the integral is the exchange energy, with exchange constant  $A$ ; this term favors homogeneous magnetization in the sample. The second term is the magnetocrystalline anisotropy with constant  $K$ , which favors specific orientations of the magnetization. The third term corresponds to the Zeeman energy, which favors magnetization aligned with the external magnetic field  $H_z$ :  $M_s$  is the saturation magnetization and  $\mu_0$  is the permeability of the vacuum. The last term in Eq. 1 represents the demagnetization energy; it captures the long-range dipole-dipole interactions between different regions of the sample:

$$E_{\text{dd}} = -\frac{\mu_0 M_s^2}{8\pi} \int_{V \times V'} \mathbf{m} \cdot \left[ \nabla \nabla' \frac{1}{|\mathbf{r} - \mathbf{r}'|} \right] \cdot \mathbf{m}' d^3 \mathbf{r} d^3 \mathbf{r}'. \quad (2)$$

where  $\mathbf{m}'$  is the magnetization at position  $\mathbf{r}'$ .

The macrospin approximation corresponds to  $A \rightarrow \infty$ , so that the sample magnetization rotates uniformly. In this case,  $\mathbf{m}$  and  $\mathbf{m}'$  can be factored out of the integrals. The dipole-dipole interaction then simplifies to  $E_{\text{dd}} = \frac{1}{2} \mu_0 M_s^2 t \Omega \mathbf{m} \cdot \mathbf{N} \cdot \mathbf{m}$ , where the demagnetizing tensor  $\mathbf{N}$  is defined to be

$$\mathbf{N} = \frac{1}{4\pi V} \int_{V \times V'} \nabla \nabla' \frac{1}{|\mathbf{r} - \mathbf{r}'|} d^3 \mathbf{r} d^3 \mathbf{r}'. \quad (3)$$

For very thin and extended films ( $\Omega \rightarrow \infty$ ,  $t = 0$ ) the off-diagonal components of  $\mathbf{N}$  tend to zero and the diagonal terms approach  $N_{zz} \rightarrow 1$ ,  $N_{xx} \rightarrow 0$ ,  $N_{yy} \rightarrow 0$ . In

this limit, the magnetostatic energy density simplifies to  $E_{dd} = \frac{1}{2}\mu_0 M_s t \Omega m_z^2$ , and the in-plane components of the magnetization ( $m_x, m_y$ ) are assumed to have negligible contribution to the magnetostatic energy.

Summarizing, in the macrospin model for thin and extended films, the magnetic energy reduces to  $E_m$ , defined as:

$$E_m = V \left[ \frac{\mu_0 M_s^2 m_z^2}{2} - K m_z^2 - \mu_0 H_z M_s m_z \right] \quad (4)$$

where  $m_z$  can have values between  $\pm 1$  and the components  $m_x$  and  $m_y$  no longer play a role. An important conclusion of this work is that even in cases of very small aspect ratio  $t/\sqrt{\Omega}$  this approximation is invalid, resulting in an underestimation the value of the energy barrier.

To calculate the MEPs associated with the full magnetization energy (1) and thereby determine the corresponding transition states and energy barriers, we utilize the String Method in conjunction with OOMMF [9]. We use 100 images between the two energy minima and reparametrize the string every 40 ps. Our initial guess path passed through a fully randomized magnetization configuration and was allowed to evolve according to the String Method prescription to its minimal energy path. Details are presented elsewhere [10–12].

Using this approach, we studied circular and square layers of thickness  $t = 1.6$  nm for a variety of diameters and side lengths  $L$  (the area  $\Omega$  is of order  $L^2$ ). We consider a material with saturation magnetization  $M_s = 713 \times 10^3$  A/m, exchange constant  $A = 8.3 \times 10^{-12}$  J/m, and anisotropy constant  $K = 403 \times 10^3$  J/m<sup>3</sup>—parameters similar to those of Co/Ni thin film nanomagnets studied experimentally in Refs. [13–15]. A constant field perpendicular to the film  $\mu_0 H_z$  was applied with a maximum magnitude equal to the coercive field, defined by  $\mu_0 H_K \equiv (2K - \mu_0 M_s^2)/M_s = 0.245$  T. Any finite external field will break the degeneracy between the two lowest lying magnetization states ( $m_z = \pm 1$ ). Any field larger than  $H_K$  will deterministically switch the magnetization, owing to an induced instability of the higher-lying in energy metastable (for  $H < H_K$ ) state.

We investigate the transition from the metastable state (hereafter that with downward magnetization) to the ground state (upward magnetization) and compare with the results from the macrospin model in which we use  $N_{zz} = 1$  except when indicated otherwise. A typical result is presented in Fig. 1 where the reversal can be seen to occur by propagation of a Bloch wall across the sample.

The field dependence of the activation energy is shown in Fig. 2. As expected, the activation energy decreases as the field approaches the coercive field.

The activation energy of the macrospin model ( $U_m$ ) can be obtained using Eq. (4). We first find the transition state by solving  $\frac{dE}{dm_z} = 0$ ; we find that the transition occurs at  $m_z = -H_z/H_K$ . The difference in energies between the transition state  $m_z = -H_z/H_K$  and the

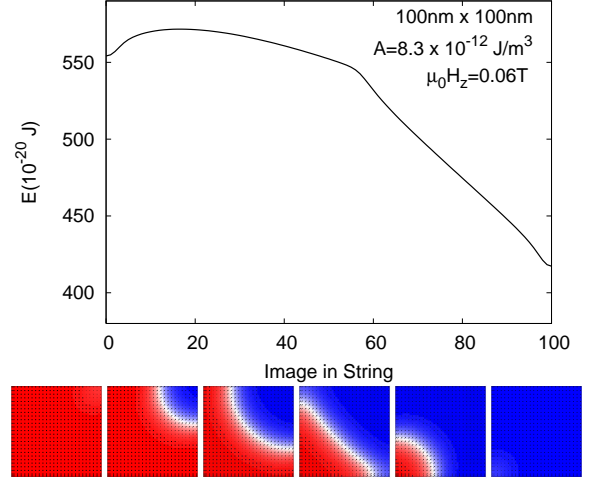


Figure 1: Images of the minimum energy path. Images shown are at locations 0, 20, 40, 60, 80, 100 in the string. Red and blue (light and dark) represent downward and upward magnetization respectively. Reversal occurs by nucleation of a domain on one corner, and propagation of a domain wall across the material. The transition state is located close to image 20. The curve presents a kink near the 55th image. This occurs when the traveling domain wall reaches the opposite corners of the element and this feature has no effect on the magnitude of the transition rate.

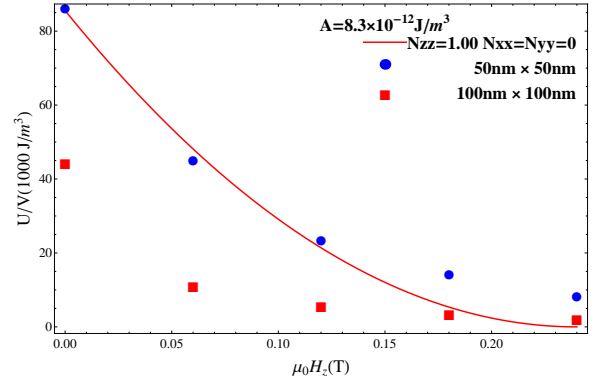


Figure 2: Field dependence of activation energy for elements with two different sizes. The smaller samples follow more closely the predictions of the usual macrospin model ( $N_{zz} = 1$ ). For large samples, it can be seen that the activation energy is lower than that predicted by the macrospin model ( $N_{zz} = 1$ ) for a large range of values of the external field. In both cases the small value of  $A$  permit nonuniform magnetization configurations and the smallest sample behaves more as a macrospin.

metastable state  $m_z = -1$

$$U_m = \frac{\mu_0 M_s H_K V}{2} \left( 1 - \frac{H_z}{H_K} \right)^2. \quad (5)$$

This relation is shown in Fig.2 and compared to our numerical results. For large samples the activation energy is clearly lower than the prediction of the macrospin model,

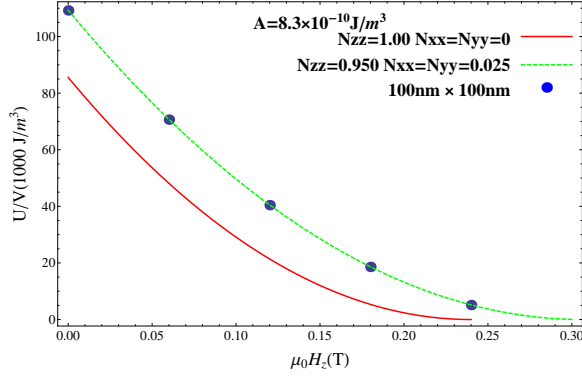


Figure 3: Comparison of two versions of the macrospin model:  $N_{zz} = 1$  corresponds to the commonly used thin film limit and  $N_{zz} = 0.95$  is a film with finite aspect ratio. Blue circles are calculated with the string method for a very large exchange constant.

as the macrospin does not account for spatial variation of the magnetization.

Two additional points need to be made regarding the way the energy barrier changes with the size of the element. First, we verified that the activation energy barrier is independent of the cell size used in the numerical integration scheme once the cells become smaller than the exchange length; this is a standard requirement of numerical micromagnetics. Therefore we conclude that our numerical results, such as those shown in Fig. 2, are not affected by numerical artifacts induced by changing the relative length scales of the system. Second, an effective reduction on the element size can be achieved by increasing the exchange constant to a large value ( $A = 8.3 \times 10^{-10} \text{ J/m}$ ). In this limit our result should approach the macrospin model even in our largest samples. The results are shown in Fig. 3, where the activation energy is compared to two versions of the macrospin model with different magnetostatic tensor components. Our results indicate that merely increasing  $A$  is not sufficient to bring the macrospin model into agreement with results found using the String Method. A further refinement of the magnetostatic energy term, in which the film is not treated as an infinite plane, is necessary. In this case, the demagnetization tensor is calculated using formulas due to Newell [16] for values  $t = 1.6 \text{ nm}$  and  $L = 100 \text{ nm}$ . Using these results yields a good agreement. This shows that in the macrospin model finite size effects are important even for very small aspect ratio ( $t/\sqrt{\Omega}$ ) thin film geometries. It must be emphasized that the gain in accuracy is obtained without a significant increase in computation time.

The finite size effect in the limit of large  $A$  can be explained as follows: if the lateral sample dimensions are comparable with the domain wall width, there is a buildup of surface charge in the lateral faces of the sample as the magnetization reverses; the sample is effectively a finite rectangular box. For intermediate values of  $A$ , such that the film can be considered to be wide

in the plane but vertically thin (when compared to the exchange length), the domain wall width becomes much smaller than the lateral dimensions and the wall does not intersect with the sample sides and produce no surface charges. Consequently, there is no contribution to the magnetostatic energy and the sample is effectively an infinite plate. In the infinite plate limit, Gioia and James [17] have argued that the magnetostatic energy can be absorbed into an effective crystalline anisotropy  $K' = (K - \frac{\mu_0 M_s^2}{2})$ .

Size effects on the activation energy in square geometries are summarized in Fig. 4, where two regimes can clearly be identified. For small samples, the activation energy increases with the size of the element; here the macrospin model holds. Beyond a certain size ( $\sim 50 \text{ nm}$ ), however, the activation energy becomes essentially constant. For large elements, the radius of the reversed nucleus is independent of the element size. For all sizes considered, the reverse domain resembles a circular region with domain walls making right angles with the sample's edge (see second image at Fig. 1). At a given configuration Eq. (1) can be approximated as the sum of three dominant terms: a switched domain with area  $\Omega_1 = (\pi R^2/4)$  with energy density per unit area  $\xi_1$  approximate to  $t \left( \frac{\mu_0 M_s^2}{2} - K - \mu_0 H_z M_s \right)$ ; an unswitched domain with downward magnetization of area  $\Omega_2 = \Omega - \Omega_1 = \Omega - \pi R^2/4$  and surface energy density  $\xi_2 \approx t \left( \frac{\mu_0 M_s^2}{2} - K + \mu_0 H_z M_s \right)$ ; and the domain wall of length  $s_3 = 2\pi R/4$  with a linear energy density per unit length  $\lambda_3 \approx 4t\sqrt{AK'}[8]$ . The total energy  $\xi_1\Omega_1 + \xi_2\Omega_2 + s_3\lambda_3$  is maximum for  $R^* = 39 \text{ nm}$ , with an activation energy of  $U \approx 16 \times 10^{-20} \text{ J}$ . This is a good approximation to the energy plateau presented in Fig. 4. Our estimate for  $R^*$  predicts to good approximation the onset of the plateau region in the activation energy: the samples must be large enough to accommodate the nucleus of size  $R^*$  at a distance of at least a few exchange lengths from the corners of the sample. A direct measurement from the numerical magnetization configuration gives  $R^* = 37 \text{ nm}$ .

The width of the domain wall is expected to be  $2\sqrt{A/K'} = 20 \text{ nm}$ ; we obtain a numerical value of  $16 \text{ nm}$ . We expect that the narrowing of the domain wall is the result of dipole-dipole interactions at the interface between the two regions. Since the magnetostatic interaction favors antiparallel configurations, the spatial rate of twist perpendicular to the domain wall increases. The increase in exchange energy is compensated by a decrease of magnetostatic energy.

The optimum radius  $R^*$  can be obtained from the above prescription to be:

$$R^* = l_{\text{ex}} \frac{M_s}{H_z} \sqrt{Q - 1} \quad (6)$$

where  $l_{\text{ex}} = \sqrt{\frac{2A}{\mu_0 M_s^2}}$  is the exchange length and  $Q = \frac{2K}{\mu_0 M_s^2}$  is the uniaxial material parameter. The optimum

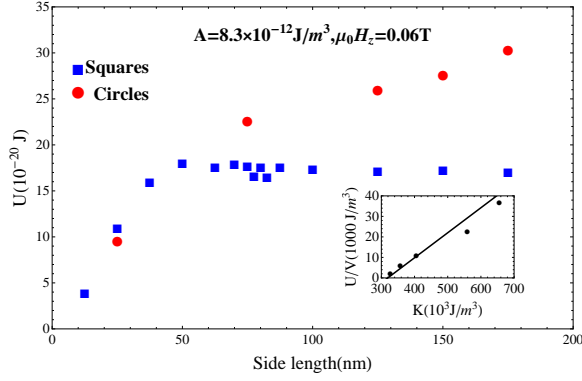


Figure 4: Activation energy for square samples (blue/dark) and circular samples (red/light). Inset: energy barriers for a square of side 100 nm for different values of  $K$ , the points are obtained with the string method and the line obeys Eq.(7).

radius depends on  $H_z$  and diverges as  $H_z \rightarrow 0$ . This is reasonable since in the absence of an external field there is no preferred magnetization direction, and so the energy barrier is produced by a straight wall parallel to one of the sides of the sample. However, in order to obtain a reasonable estimate of the energy barrier we need to impose two conditions. First, we must guarantee that the switched domain fits in the sample by  $R^* < L$ ; second, we require the domain wall width to be smaller than the square side  $2\sqrt{A/K'} < L$ . Rewriting  $2\sqrt{A/K'}$  as  $\frac{2l_{ex}}{\sqrt{Q-1}}$  and using Eq. (6) we arrive at the following condition on the external magnetic field for our model to be valid:  $H_z > 2M_s \left(\frac{l_{ex}}{L}\right)^2$ . For example, with  $L = 50$  nm, the condition is  $\mu_0 H_z > 0.02$  T. When this condition is satisfied the activation energy can be estimated by

$$U = \pi l_{ex}^2 K' t \frac{M_s}{H_z} = \pi A t \left( \frac{2K}{\mu_0 M_s^2} - 1 \right) \frac{M_s}{H_z}. \quad (7)$$

The behavior of the energy barrier for square samples results from the presence of sharp corners that favor nucleation. In contrast, circular shapes do not present such behavior. Fig. 4 shows the computed activation energies for circular samples as a function of in plane diameter. The activation energy continues to increase as the diameter increases. As a result circular samples become more thermally stable for increasing size.

We tested the validity of Eq. (7) by varying the value of the magnetocrystalline anisotropy. The results are represented on the inset of Fig.4. There is a clearly increasing

and nearly linear behavior, as predicted by the analytical expression.

In conclusion, we used the String Method to determine activation energies for thermally induced magnetization reversal and compared the results to a macrospin model. Our results indicate that finite size effects on the macrospin model are important even for very thin samples. The energy barrier of the macrospin model can be calculated more accurately and at no additional computational cost by using the full demagnetization tensor. In addition, the activation energy for square samples as a function of size displays a transition from linear dependence to a constant value at a critical size. We predict that for circularly samples the activation energy will continue to increase beyond a critical size, albeit more slowly. We have also provided an analytic estimate for the activation energy for nonuniform magnetization reversal in nanomagnets with perpendicular anisotropy, which can guide experiment and memory device development.

### acknowledgments

This research was supported by NSF-DMR-100657, PHY0965015, NSF-DMS-0708140, ONR-N00014-11-1-0345, and NSF PHY-0965015.

### Appendix

The magnetostatic tensor has been calculated by Newell [16]. Using Gauss' Law Eq. 3 can be transformed into

$$\mathbf{N} = -\frac{1}{4\pi V} \int_{S \times S'} \frac{1}{|\mathbf{r} - \mathbf{r}'|} \hat{\mathbf{n}} dS \hat{\mathbf{n}}' dS'. \quad (8)$$

where  $S$  is the surface enclosing the sample and  $\hat{\mathbf{n}}$  is the unit vector normal to the surfaces of the sample. The components of the magnetization tensor are obtained by selecting the appropriate surfaces of orientation, e.g. the  $N_{xy}$  term is obtained by using the sides where  $\mathbf{n} dS = \hat{\mathbf{x}} dy dz$  and  $\mathbf{n}' dS' = \hat{\mathbf{y}} dx dz$ . Notice that the trace of the integrand in Eq. 3 can be calculated using  $-\nabla \cdot \nabla' \left( \frac{1}{|\mathbf{r} - \mathbf{r}'|} \right) = \Delta \left( \frac{1}{|\mathbf{r} - \mathbf{r}'|} \right) = 4\pi \delta^3(\mathbf{r} - \mathbf{r}')$ , where  $\Delta$  denotes the Laplacian. It follows that  $\text{Tr}[\mathbf{N}] = 1$  for a body of arbitrary shape.

[1] C. A. Ross, H. I. Smith, T. Savas, M. Schattensburg, M. Farhoud, M. Hwang, M. Walsh, M. C. Abraham, and R. J. Ram, *Journal of Vacuum Science & Technology B: Microelectronics and Nanometer Structures* **17**, 3168 (1999).

[2] A. Brataas, A. D. Kent, and H. Ohno, *Nature Materials* **11**, 372 (2012).  
 [3] H. Braun, *Physical Review B* **50**, 16501 (1994).  
 [4] H. Kramers, *Physica* **7**, 284 (1940).  
 [5] K. Martens, D. L. Stein, and A. D. Kent, *Physical Review*

- B (Condensed Matter and Materials Physics) **73**, 054413 (2006).
- [6] W. E. W. Ren, and E. Vanden-Eijnden, Journal of Applied Physics **93**, 2275 (2003).
  - [7] P. Hänggi, P. Talkner, and M. Borkovec, Reviews of Modern Physics **62**, 251 (1990).
  - [8] A. Hubert and R. Schafer, *Magnetic domains: the analysis of magnetic microstructures* (Springer, 1998).
  - [9] M. J. Donahue and D. Porter, Interagency Report NISTIR 6376, National Institute of Standards and Technology, Gaithersburg (1999).
  - [10] W. E. W. Ren, and E. Vanden-Eijnden, Physical Review B **66**, 052301 (2002).
  - [11] W. E. W. Ren, and E. Vanden-Eijnden, The Journal of Chemical Physics **126**, 164103 (2007).
  - [12] G. D. Chaves-O'Flynn, D. Bedau, E. Vanden-Eijnden, A. D. Kent, and D. L. Stein, IEEE Transactions on Magnetics **46**, 2272 (2010).
  - [13] D. Bedau, H. Liu, J. Bouzaglou, A. D. Kent, J. Z. Sun, J. A. Katine, E. E. Fullerton, and S. Mangin, Applied Physics Letters **96**, 022514 (2010).
  - [14] D. Bedau, H. Liu, J. Z. Sun, J. A. Katine, E. E. Fullerton, S. Mangin, and A. D. Kent, Applied Physics Letters **97**, 262502 (2010).
  - [15] H. Liu, D. Bedau, J. Z. Sun, S. Mangin, E. E. Fullerton, J. A. Katine, and A. D. Kent, Physical Review B **85**, 220405 (2012).
  - [16] A. J. Newell, W. Williams, and D. J. Dunlop (1993).
  - [17] G. Gioia and R. D. James, Proceedings of the Royal Society of London. Series A: Mathematical, Physical and Engineering Sciences **453**, 213 (1997).